ô OPEN ACCESS

Review of Vent Systems of Space Vehicle, Spacecraft and Aircraft

R. C. Mehta[1*]

[1]Department of Aeronautical Engineering, Noorul Islam Centre for Higher Education, Kumaracoil 629180, India

Abstract	Review Article

The main focus of the review article is to present the vent system of space vehicle and spacecraft. Quasi-one dimensional, quasi-steady and isentropic analytical and computational fluid dynamics equations are employed to compute differential pressure inside the compartment. Discharge characteristics of vent system depend on geometry, location of vent and external environment. An inverse analysis is performed to estimate the discharge coefficient using measured and computed compartment differential pressure time history. The reconstructed differential pressures of the compartment are compared with pre- and post-flight data. The differential pressure and the rate of pressure drop in the compartments are analysed via isentropic equations. A numerical scheme based on compressible gas dynamics relation is discussed for pressurization of aircraft cabin. The vent valve with a spring loaded butterfly valve can be evaluated using the isentropic relations.

Keywords: aircraft; butterfly valve; CFD; depressurization; discharge coefficient; inverse problem; orifice; re-entry; vent system; space vehicle; spacecraft.

1. INTRODUCTION

The inside pressure of a payload fairing PLF of a space launch vehicle SLV, compartments of a spacecraft and cabin pressure at take-off of an aircraft is at the atmospheric condition. The outside atmospheric pressure decreases rapidly during the ascent period of the flight, resulting a build-up of pressure differential between inside and outside wall. Venting analyses simulate the time-dependent flow of multi compartment inside the space vehicle, spacecraft and aircraft.

The PLF of a SLV requires venting so as to prevent excessive internal pressure build-up which can lead to a structure failure. The differential pressure inside the PLF depends mainly on effective compartment volume to be evacuated, location, size and type of vent system, boundary layer around vent and trajectory of the SLV.

The SLV and the spacecraft contain several inter connected compartments such as insulation panels, honey comb structure and inter stage compartment etc. The base thermal shroud is needed venting in order to avoid busting caused by the pressure pulse at the time of ignition of solid motor. It is important to mention here that structure failure may become due to placing vent hole ahead of protuberance or along the shock wave that will cause excessive internal pressure build-up in the compartment.

Re-pressurization is required during the re-entry of a spacecraft in order to reduce the pressure differential across the wall. The rate of change of internal pressure with time is another important design requirement of vent system in order to avoid malfunction of electronic components. The vent system of the SLV must also satisfy pre-launch purging, air conditioning and contamination of spacecraft.

Passenger aircraft requires maintaining required pressure differential inside the cabin during take-off, cruise and landing. Figure 1 depicts typical configurations of SLV, spacecraft and aircraft. Figure 2 illustrates the flight trajectory of SLV from lift-off to injection of spacecraft to the designated orbit and also depicts the re-entry sequences of spacecraft till touch down to ground.

2. Earth Atmosphere

Figure 3 depicts the Earth atmosphere from sea level to 10^5 m which is classified in the troposphere, the stratosphere, the mesosphere, and the thermosphere. An international tropical reference atmospheric up to 10^5 m has been tabulated by Anathasayanam *et al.,* [1].

Commercial airliners typically cruise at altitudes of 9 – 12 km which is in the lower reaches of the stratosphere in temperate latitudes. The International Astronautical Federation (IAF) defines the Kármán line as space beginning 10^4 m above the Earth's mean sea level. The Kármán line is an attempt to define a boundary between Earth's atmosphere and outer space.

The troposphere (0 – 20 km) is the first and lowest layer of the atmosphere of the Earth. The maximum air pressure is at sea level and decreases at high altitude because the atmosphere is in hydrostatic equilibrium. The tropopause is the atmospheric boundary layer between the troposphere and the stratosphere. The stratosphere (20 – 50 km) is the second layer of the atmosphere of the Earth, located above the troposphere and below the mesosphere. The stratosphere is an atmospheric layer composed of stratified temperature layers. The mesosphere (50 – 80 km) is the third layer of the Earth's atmosphere, directly above the stratosphere and directly below the thermosphere. In the mesosphere, temperature decreases as altitude increases. The thermosphere (80 – 1000 km) is the layer in the Earth's atmosphere directly above the mesosphere and below the exosphere. The exosphere is a thin, atmosphere-like volume surrounding the Earth's. The exosphere is the uppermost layer, where the atmosphere thins out and merges with outer space. It is located directly above the thermosphere.

3. Space Launch Vehicle

During the atmospheric flight, the PLF of a SLV requires venting in order to prevent excessive differential pressure build-up, which may be detrimental to the structure. In order to analysis the venting process and predict the time history differential pressure reasonably for the design, a compressible flow loss coefficient is essential for the mass flux calculation.

International reference catalog [2] to various SLV tabulated the maximum differential pressure and rate of change of pressure inside the fairings. The NASA monograph [3] describes the design criteria of compartment venting for space vehicles during ascent and re-entry period.

Flow areas for series and parallel compartment venting to satisfy pressure differential requirements have been studied by Kirby and Ivy [4]. Experiments were conducted by John and Jones [5] in the 8 × 6 ft supersonic wind tunnel of the NASA Lewis Research Centre to find the effective discharge coefficient for the venting analysis and application of the Titan/Centaur launch vehicle. It is very difficult to obtain the discharge coefficient from experiments. Fay and Hengel [6] analyzed the flow through the vent connecting the multi-compartment using a quasi-steady isentropic equation with empirical discharge coefficient.

An analytical approach of the discharge process of a compartment into a decreasing time-dependent pressure environment has been published by Sanz-Andres et al., [7]. A closed-form expression for the isothermal [8] venting has been presented using small time-steps during the short time of depressurization. Dykhuizen et al., [9] have derived analytical solutions to calculate the internal pressure of vented enclosure during launch.

The effective discharge coefficient for multi-row vent-holes on the payload fairing of Titan IV launch vehicle has been numerically obtained using three-dimensional Computational Fluid Dynamics (CFD) technique by Huseman and Chern [10]. The discharge coefficient of vent holes has been obtained for a range of external flow Mach numbers and internal-to-external pressure ratios applicable to Titan IV flight trajectory. Brower [11] has reported the internal payload fairing compartment pressure inside the Titan launch vehicle.

Moraes and Pereira [12] have presented verification of the computed and measured differential pressure inside the satellite vented compartment of the Brazilian satellite launch vehicle. The external pressure in the vicinity of the vent holes is taken by them from the wind-tunnel data.

Quasi-one-dimensional compressible inviscid equations are solved by Mehta [13] using a finite volume technique to compute differential pressure inside the heat shield taking into consideration changing external conditions at the launcher altitude changes. The computational cost of a typical discretiztion of time-dependent three-dimensional full Navier-Stokes equations is generally very large, due to simulation of the flow field at each time of trajectory of the launch vehicle.

The vent analysis becomes more critical for large or complex for launch vehicle [14, 15]. Design and development of depressurization system of launch vehicle fairing is evaluated by Iqbal et al., [16]. Thermodynamics study of compartment venting has been carried out using numerical method by Benavente [17]. The performance characteristics of a vent valve with a spring-loaded door has been evaluated for Korea space launch vehicle-II by Oh et al., [18]. Singh [19] has carried out venting analysis for heat shield of SLV using isothermal relation. Numerical simulation of depressurization in multi-compartment has been carried using quasi-one-dimensional method [20]. Analysis of payload compartment venting of SLV is carried out by Mehta [21] employing isentropic flow equations. Compartment venting of Ares 1 has been carried out by Wang and Amer [22]. Ares I-X upper stage simulator compartment pressure comparisons during ascent

period is performed by Downs *et al.,* [23].

4. Spacecraft

The pressure inside the compartment of the space capsule at the time of atmospheric reentry is at low pressure level. As the space capsule started entering in the Earth's atmosphere, the ambient pressure increases rapidly as a flight altitude decreasing, causing a built up of differential pressure across the compartment. The rate of re-pressurization and compartment differential pressure can cause structural damage to the space capsule and malfunctioning of the electronic components. Therefore, the re-pressurization of the unsealed compartments on the space capsule at the time of reentry into the Earth's atmosphere is essential and must be analysed to meet the design constrained. One of the design requirements is to keep the compartment pressure as close to the ambient pressure. The contamination limits can too restrict air ingesting and temperature limits of heat sensitive electronic equipment. The vent holes of the space capsule requirement must also compatible to satisfy the pre- or post-flight purging, vent and drain system requirements.

The vent holes of the space capsules must satisfy the design limits of the ascent and descent phase since the space capsule is kept inside the payload shroud as schematically illustrated in Fig. 2 (a). The vent holes in the space capsule are provided in the base plate region that will satisfy both depressurization and re-pressurization conditions during the ascent and descent period respectively.

Re-pressurization of the unsealed compartments on the Orion Crew Exploration Vehicle's Crew Module during re-entry into the Earth's atmosphere has been analysed by Smith [24]. Stardust back shell and back interface plate design verification tests have been carried out in the NASA Ames arc jet facilities by Johnson *et al.,* [25]. Base vent assembly for re-entry has been patented by Charette and Yales [26]. Spacecraft compartment is carried out by Scialdone [27]. Compartment venting during atmospheric re-entry of the space capsule [28] is carried out using isentropic relations.

5. Sounding Rocket

Vents are also needed in sounding rocket [29, 30] to prevent the differential pressure build up inside compartments and fins as shown in Fig. 4. The CFD analysis of flow field and variations of pressure coefficient is required to determine the location and size of vent hole.

6. Space Shuttle

Experimental studies were carried out by Mironer and Regan [31] to determine the venting design criteria for the space shuttle payload, using a nominal ascent trajectory, and payload bay pressure profile.

Murri [32] has experimentally studied venting design criteria for space shuttle payloads using worst case ascent phase trajectory, and payload bay pressure profile. They obtained a single curve that indicates the maximum differential pressure which can be expected for a given vent hole diameter. More complex configurations such as the space shuttle require venting in which a quantity of small experimental package may be kept in a large payload container within a cargo bay and exposed to various conditions of the ascent and reentry trajectory conditions.

Flight performance of vent of space shuttle orbital is evaluated by Lutfi *et al.,* [33]. A post flight analysis of the space shuttle showed that the differences between the pre-flight prediction and measured values differential pressure were primarily due to difference between external pressures, which are based on subscale wind-tunnel test data, and the actual vehicle external pressure measured during the flight. Most of the predictions of the discharge coefficient are based on the flight derived vent port pressure coefficients since the wind tunnel does not adequately define the orbiter ascent pressure environment. Figure 5 shows various compartments of space shuttle orbiter that needs vent to relieve differential pressure build up during ascent phase of flight of space shuttle. Figure 6 shows differential pressure in the payload bay during the ascent period of the space shuttle.

7. Honey Comb Structure

A honeycomb sandwich structure is made of a honey comb core bonded to skin of spacecraft. Vented honey comb structures are perforated, which air can flow from cell to cell at a rate corresponding during the ascent phase of a SLV and spacecraft. The changes in pressure within the panel should occur at a rate corresponding to the external pressure variation during flight.

Epstein and Ruth [34] have conducted experiment on honeycomb sandwich structures and observed that failures occur due to internal pressure when the external environment is reduced in ambient pressure. They recommended that the honeycomb sandwich structure for space system to be adequately vented in order to minimize the likely hood of failure. A n implicit method for numerically stiff venting problem s in honeycomb and other multicell configurations is stu died by Ahn [35].

8. Aircraft

Aircraft has a pressurization system that constantly pumps fresh air in the cabin. The maximum pressure differential is a structural limit that restricts the aircraft maximum certified flight altitude. The automatically controlled valves are opened when pressure has to be reduced. The bleed air produced by gas turbine engines is used for the aircraft's pressurization system; the switch controlling is kept on.

Figure 7 shows the variation of pressure with altitude. It reveals that the pressurization of cabin is essential for safety of passenger aircraft. Figure 8 depicts the sequence of pressurization system marked with 1 – 4 in the diagram to maintain required differential pressure inside the aircraft.

Outside air enters engine and compressed air is injected into the fuselage with proper conditioning. Cool air is circulated in cabin, creating an ambient environment. Outflow valve ensures proper pressure.

Analysis of aircraft fuel tank vent system is required for proper function of fuel supply system. A systematic model of sudden depressurization of cabin is required to control the depressurization. Many closed-form solutions for isothermal, polytropic, and isentropic decompression were derived for re-pressurization for aircraft and spacecraft by Mavriplis [36]. Analytical solutions to compute the decompression of pressurized aircraft cabin are derived by Pagani *et al.,* [37] under constant ambient pressure conditions and used for computing structural loads on hinged panes. Venting analysis of a Boeing 747 aircraft fuel tank has been carried out by Jensen [38]. It is worth to mention here the major difference between the depressurization process of aircraft and launch vehicle is that in the case of aircraft the back pressure is equal to the atmospheric pressure of ambient air and remains constant during the process of decompression but in the case of space launch vehicles the ambient pressure falls rapidly. The temporal change of the cabin air pressure van be estimated from an integral mass balance equation described in the following section. The discharge coefficients were obtained through measurements, CFD analyses by Breard *et al.,* [39] or sensitive analyses by Daidzic and Simones [40].

9. Compartments of SLV, Flow Field and Pressure Distribution Over SLV

The compartment vent system of SLV is illustrated in Fig. 9. Air flow path through different compartment is illustrated from PLF to flow out through vent holes. Inter compartment flow passes through the wire tunnel. The vent system includes the openings between compartments and unplanned leakage areas as the joint between the heat shield and cylinder. The fire in the holes are typical SLV staging separation of strap on. In the case of multi compartment vent, the disturbance of the flow field is less pronounced but can have an effect on the mass flow rate through the vent. The Mach contour over the SLV for transonic and supersonic speeds is depicted in Fig. 10 (a) and (b), respectively. It can be seen from the figure that the external flow field environment varies not only with flight time but also with position over the SLV. The external flow field over SLV that generates during atmospheric flight produces a pressure distribution over the structure and calculates the rates of energy and mass transfer through the vent.

Flow field over the protuberance computed at Mach 1.2 and 1.6 is shown in Fig. 11. A shock wave is formed ahead of the protuberance that will generate high external pressure over the SLV if the vents are located and may become detrimental to SLV. Figure 12 (a) and (b) describes pressure distribution over the SLV for transonic and supersonic Mach numbers. The movement of terminal shock is computed over SLV in transonic Mach number range in [41]. The variation of pressure coefficients [42] along the SLV at transonic and supersonic Mach number are numerically computed. The detailed flow field is simulated from CFD [43].

The flow rates through vents are very sensitive to variations of pressure at the vent. The location of terminal shock waves extremely essential, because of variation of Mach number during flight, the shock waves appear to move, and their detailed position may depend upon the flight trajectory. These computed pressure profile on the SLV an important input to decide vent system location and size of vent hole and selecting proper discharge coefficient C_D of the vent hole.

10. Jet Emanating from Vent to Ambient

The convergent nozzles operating under varying pressure ratios. The values of stagnation pressure p_c and stagnation temperature T_c will be maintained constant at the inlet of the nozzle. It involves variation of back pressure p_a and exit plane of the convergent nozzle p_e. The various pressure operating conditions p_b/p_e are shown in Fig. 13 as a function of increasing pressure ratios p_b/p_e. Points 1 represent $p_a/p_c = 1$ corresponds to no flow. Points 2 and 3 correspond to decreasing value of p_a/p_c, an increase the flow rate. Further reduction in p_a reaches a critical pressure ratio $p^*/p_c = 0.5283$ and $M_e = 1$ as point 4 and chocked flow or maximum mass flow rate. Further reduction of p_a/p_c shows identical flow of point 4. If the emanating jet from vent is subsonic the disturbance it induces in the surrounding flow field can in turn effect the strength of the jet. Figure 14 shows variation of p_c/p_e vs p_b/p_e, mass flow rate and p_b/p_e vs mass flow rate. Maximum flow rate occurs at p^*/p_c.

Figure 15 (a) exhibits schematic sketch of field shock wave boundary layer interaction. Flow field of vent inter acts with boundary produces a complex flow field as seen in the figure. The presence of flow through the vents may modify the external pressure variation. Figure 15 (b) reveals the complexity of flow field around a vent because of supersonic external flow and flow leaving the vent. The exiting jet interacts with the external flow to form separated flow regions forward and aft of the vent. These separated flow attributes a pressure alter in the outside flow field.
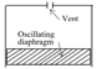
11. Discharge Coefficient

The discharge coefficients C_D has been defined for a range of external flow Mach number over SLV and differential pressure ratios inside the PLF of the SLV. The C_D used should be applicable in terms of orifice Reynolds number and pressure ratio across the orifice. The local external flow conditions of local Mach number, pressure, and boundary layer should be accounted for in orifice flow analysis. In designing vent system which will meet this requirement, it is necessary to know discharge characteristics of the vent opening as they affected by both geometry of the opening and the external environment. The CD are obtained from wind tunnel as a function of Mach number and vent diameter in [44, 45].

12. Vent System

The use of more than two vents exhausting flow outside of the vehicle and located symmetrically around a given circumference of the compartment is recommended. Figure 16 shows a PLF of SLV and vent without valve. Various butterfly valves are shown in Fig. 17. Table 1 shows the characteristics of orifice, tube, diaphragm, butterfly valve and one-sided valve. The discharge coefficients depend on the type of vent.

Table 1 Characteristics of vent system

Type	Descriptions	Diagram
Orifice	Simple, Fixed area	
Tube, pipe or duct, bicycle tube valve	Simple routine flow path, Fixed area; accuracy of discharge coefficient	
Frangible diaphragm	Simple; operated as an on/off valve, Uncertain discharge coefficient;	
Mechanical operated panel (spring-loaded door)	Operated as an on/off valve which allows orifice size to change; opens on command; can be very large, may inadvertently open	
One side valve	Controlled mass flow directions; controls pressure level	

13. Calculation of Compartment Pressure Using Isentropic Relations

Using the first law of thermodynamics for an isentropic process and employing the pressure-density-temperature relationship in the form of perfect gas law, one obtains isentropic relationship [46] as a function of the internal pressure level and the velocity is a function of pressure and density [47].

The maximum mass flow rate equation [48] for choked flow is

$$\dot{m}_{max} = \frac{C_D \rho_c A \sqrt{\gamma}}{\sqrt{RT_c}} \left(\frac{2}{\gamma+1} \right)^{-\frac{(\gamma+1)}{2(\gamma=1)}} \qquad (1)$$

The maximum flow equation can be written as

$$\dot{m}_{max} = C_D a \rho_c A \left(\frac{2}{\gamma+1} \right)^{-\frac{(\gamma+1)}{2(\gamma=1)}} \qquad (2)$$

And the compartment air pressure versus atmospheric pressure ratio decrease to a critical pressure ratio [47] as

$$\frac{p^*}{p_c} = \left(\frac{2}{\gamma+1} \right)^{\frac{\gamma}{\gamma-1}} = -0.5283 \qquad (3)$$

A relatively simple expression for the rate of pressure decrease resulting from escape of air through a vent can be obtained when $p_a^* > p_c$. It is important to say that the decompression process does not depend on the ambient pressure. In the case of subcritical case the rate of discharge is proportional to the differential pressure rather than the process itself. When the time for an acoustic wave to cross the compartment is far less than the time for a change in the boundary condition, i.e., $\{(t/L)\ a\} \gg 1$. L is the characteristic length of the compartment. The problem of flow in compartment and through the vent system can be formulated as an unsteady, nonlinear, differential equation system and obtain as

$$\frac{dp_c}{dt} = \mp C_D \frac{\gamma A a}{V_c} p_c \sqrt{\frac{2}{\gamma-1} \left(\frac{p_a}{p_c} \right)} \sqrt{1 - \left(\frac{p_a}{p_c} \right)^{\frac{\gamma-1}{\gamma}}} \qquad (4)$$

Here, C_D is the discharge coefficient of the vent orifice. A is the area of the vent hole. The discharge coefficient is defined as the ratio between the actual diabatic irreversible outflow and the theoretical maximum possible or isentropic outflow. V_c is the area of the vent hole and compartment volume. The equation can be written by introducing a similarity parameter [$\tau = (A \cdot a/V_c) \cdot t$] and Equation (4) can be rewritten as

$$\frac{d\left(\frac{p_a}{p_c} \right)}{d\tau} = \mp C_D \gamma \sqrt{\frac{2}{\gamma-1} \left(\frac{p_a}{p_c} \right)} \sqrt{1 - \left(\frac{p_a}{p_c} \right)^{\frac{\gamma-1}{\gamma}}} \qquad (5)$$

In the above Eq. (5), – sign for depressurization and the + sign for pressurization. The non-dimensional τ is a characteristic time during which pressure or other boundary conditions change. A small time constant τ means a short time of decompression that is a fast decompression. The discharge coefficients used should be applicable in terms of orifice Reynolds number and pressure ratio across the orifice. The local external flow conditions of Mach number and boundary layer thickness and profile should be accounted for in the orifice flow analysis. The external pressure history in the vicinity of the vent should be calculated on the basis of the vehicle's trajectory in the atmosphere.

Equation (5) is an ordinary nonlinear differential equation. It contains the ambient pressure $p_a(t)$ as a function of time. A fourth-order Runge-Kutta method is used to compute the compartment pressure. C_D depends on the vent area, location and local Mach number. The time step in the numerical analysis should be compatible with the (V_c/Aa). The differential pressure can be calculated as

$$\Delta p = p_c - p_a \quad (6)$$

Where the Δp is differential pressure between the compartments to ambient pressure.

14. Quasi-One-Dimensional CFD Analysis of Vent of SLV

An attractive feature of the reduced-spatial dimension model is to numerically compute the pressure inside the PLF of the SLV by using the time-dependent compressible quasi-one-dimensional Euler equations. The governing fluid dynamics equations can be written in conservation law form as follows:

$$\frac{\partial U}{\partial t} + \frac{\partial F}{\partial x} + S = 0 \quad (7)$$

$$U = \begin{bmatrix} \rho \\ \rho u \\ \rho e \end{bmatrix}, \quad F = A(x)\begin{bmatrix} \rho u \\ \rho u^2 + p \\ u(\rho e + p) \end{bmatrix}, \quad S = -\begin{bmatrix} 0 \\ p\dfrac{\partial A}{\partial x} \\ 0 \end{bmatrix}$$

Where U is the vector of conserved variables and F is flux vector. S is source term due to the area variables. A is the cross-sectional area of the quasi-one-dimensional depressurization equation for the venting. It is assumed that A is a continuously differentiable function that is independent of time. Therefore, A is a function of axial distance, x and can be expressed as $A = A(x)$. The variables ρ, u, p, and e are the density, velocity, pressure and total specific energy, respectively. The equation of state for perfect gas is

$$p = (\gamma - 1)\rho\left(e - \frac{1}{2}u^2\right) \quad (8)$$

Where γ is the ratio of specific heats of air.

The numerical algorithm employs a finite volume discretization technique. The computational domain is divided into a number of small cell intervals in one-dimension. The convective flux balance over the cell is approximated by taking average flux vectors on each grid cell with its magnitude and the outer normal for its direction. The scheme is a central difference schemes on Cartesian grid. Artificial dissipation terms [49] are used to damp numerical oscillations. The spatial discretization reduces the governing equations to semi-discrete ordinary differential equations. Figure 18 shows the grid arrangement in the axial direction. The integration is carried out using three-stage Runge-Kutta time-marching method [49, 50].

The numerical scheme is validated with the experimental results of Mironer and Regan [31]. They simulated Space-Shuttle cargo-bay payload at ground using different diameter of orifice to vent out the air from the compartment. In the experiment they used a 2.831×10^{-2} m^3 tank containing air at an atmospheric conditions exhausted to a bell jar being evacuated by mechanical vacuum pump. The orifice diameter is taken about 0.625×10^{-2} m^2.

The governing equations are closed with the following boundary conditions. A symmetric condition is imposed on the center line of the payload fairing. This gives two-way venting of the compartment air to the surrounding. At the other end of the fairing i.e., at the vent whole location, ambient condition is used, based on the trajectory of the satellite launch vehicle. The ambient pressure, temperature and density are taken from the standard atmospheric data [1]. The ambient conditions of the vent depend on the trajectory of the satellite launch vehicle.

15. Estimation of Discharge Coefficient of SLV

The differential pressure can be calculated as

$$E(C_D) = \left| \Delta p_c - \Delta p_m \right| \quad (9)$$

A controlled random search CRS technique [51] has been applied for the estimation of the discharge coefficient C_D from the pressure-time history measured during the ascent phase of a SLV as well as for re-entry spacecraft. The controlled random search method does not require calculation of the sensitivity coefficient and the future-pressure information. The CRS algorithm does not need computation of derivatives but depends on function $F(C_D)$ evaluation alone. The function $F(C_D)$ is difference between measured and calculated values of the differential pressure. It works even when the differentiability requirements cannot be assured in the feasible region of variable C_D. For initiating CRS algorithm no initial guess value, except for an estimate of C_D, is required. The algorithm does not depend on the future-pressure information.

The CRS algorithm is implemented in two steps. In the first step, random feasible points generated from C_D and $F(C_D)$ are computed at each point and information stored as a matrix. The maximum and minimum values $F_M(C_D)$, $F_L(C_D)$ of $F(C_D)$ and corresponding points M and L are then identified. In the second step, these random points are manipulated iteratively to yield a better candidate for global solutions. To this extent at each iteration arbitrary distinct points are selected from matrix.

The details of controlled random search algorithm are described by Mehta and Tiwari [52] and Mehta [53]. The CRS algorithm predicts the discharge coefficient as a function of stepwise Mach number. Reconstructed differential pressures show good agreement with the numerical results. It is important to mention here that the maximum differential pressure and the rate of decrease as the differential pressure are within the permissible limits as mentioned by Isakowitz *et al.,* [2]. The volume of air to be evacuated in the heat shield of a typical launch vehicle is about 42 m^3 and the vent area is about 0.0472 m^2. The vent area is distributed as a number of circular holes. Figure 19 shows the computed and measured differential pressure variation inside PLF which employed in conjunction with Eq. (9) to estimate C_D. Table 2 shows the estimated value of discharge coefficient in the Mach number range.

Table 2 Estimated values of C_D

Mach number range	C_D
M ≤ 0.5	0.90
0.5 < M ≤ 0.75	0.70
0.75 < M ≤ 1.00	0.40
1.00 < M ≤ 1.25	0.20
1.25 < M ≤ 1.50	0.15
1.50 < M ≤ 2.00	0.10
2.00 < M ≤ 4.50	0.10

16. Estimation of Discharge Coefficient of Spacecraft

The Space capsule Reentry Experiment (SRE-1) [28] was launched by PSLV-C7 from Satish Dhawan Space Centre, Sriharikota, India on January 19, 2007 and successfully recovered on January 22, 2007. Using the inverse venting method, a prediction of discharge coefficient as described above is used in conjunction with the measured pressure inside a typical space capsule. Figure 2 (b) depicts layout of the space capsule.

Figure 20 shows the spacecraft is kept inside PLF of SLV. Figure 21 depicts various compartments of the spacecraft that requires multi-compartment analysis to compute differential pressure. Figure 22 shows honeycomb structure of spacecraft which has to be analysed in order to avoid debonding of honeycomb structure.

The capsule is having four inter connected compartments. The compartment volume V_c is about 2.265×10^{-3} m^3 and total vent hole area A_H is 2.3×10^{-3} m^2. The vent area is distributed in a ten number of circular holes in the base region of the space capsule. The pressure inside the compartment is measured using a pressure transducer during the reentry and is transmitted to the ground station through the telemetry as shown in Fig. 23. Computed and measured differential pressure variation inside spacecraft with flight time is shown in Fig. 24. Using Eq. (9), the discharge coefficient during re-entry period are estimated and depicted in Fig. 25.

17. Design of Heat Shield Latch

The structure load on the latch of heat shield as shown in Fig. 26 requires compartment pressure. The pressure variation inside the PLF during the ascent through the atmosphere generates structured loads on the latch.

$$L_1 = \int_0^L \frac{w(x)(\bar{x} - xL_2)}{x(L_2 - L_1)} dx \tag{9a}$$

$$L_2 = \int_0^L \frac{w(x)(\bar{x} - xL_1)}{x(L_2 - L_1)} dx \tag{9b}$$

Where L is length of heat shield, $w(x)$ load due to difference between outside pressure and inside pressure on unit with of element of heat shield, xL_1 and xL_2 location of front and rear latches, respectively.

Pressure equalization during lift-off in the PLF

Cooled air is disconnected at the time of lift-off to the PLF of SLV. In order to prevent containment of spacecraft, it is required to compute time required to stabilize the pressure inside the PLF employing following isentropic relation [48]:

$$t = \frac{V}{A\sqrt{\gamma R T_i \left(\frac{2}{\gamma + 1}\right)^{\frac{(\gamma+1)}{(\gamma-1)}}}} ln\left(\frac{p_f}{p_i}\right) \tag{10}$$

Most of the predictions of the discharge coefficient are based on the flight-derived vent port pressure coefficients, because the wind tunnel does not adequately define the orbital ascent pressure environment.
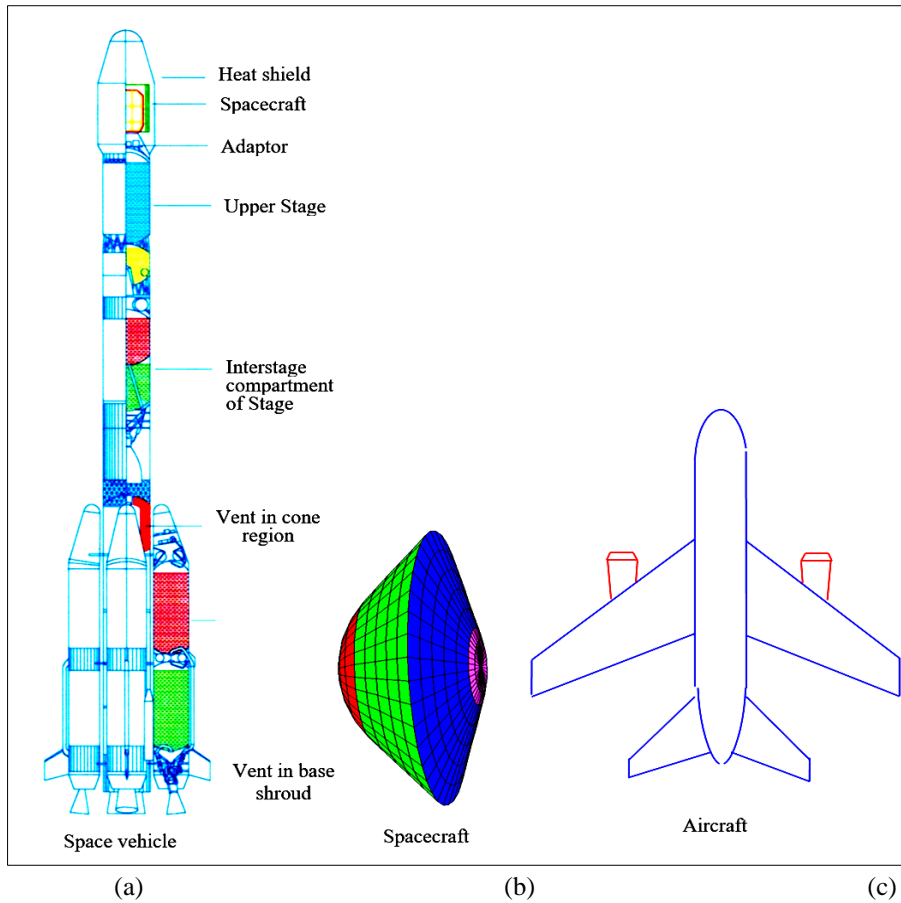
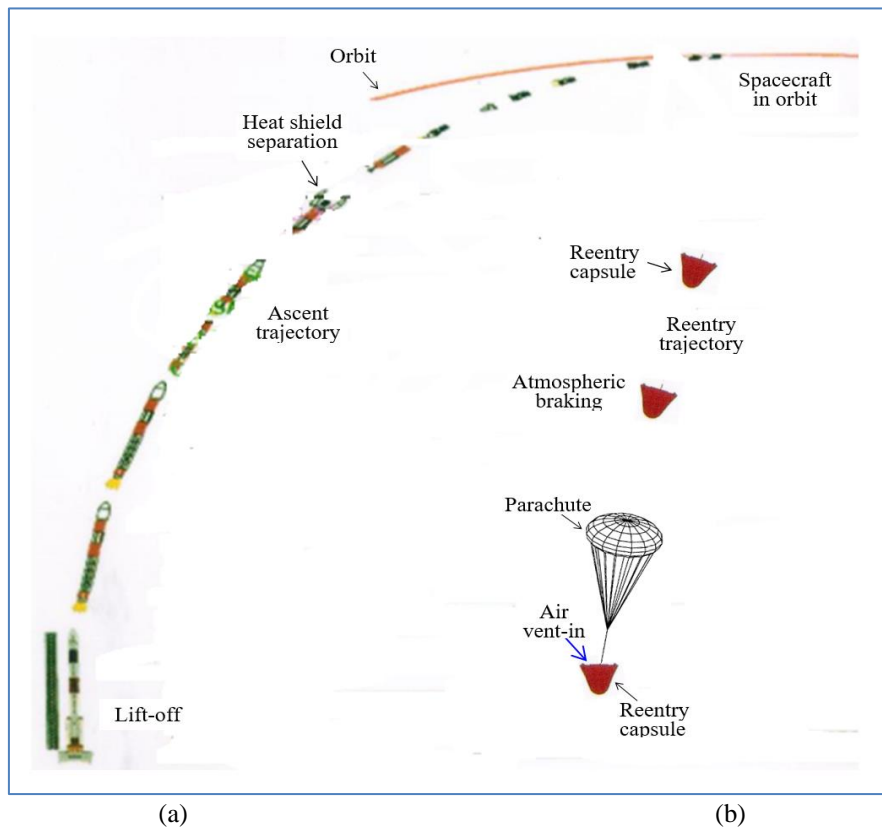**Fig. 1: Vent system for (a) space vehicle, (b) spacecraft, and aircraft (c)**

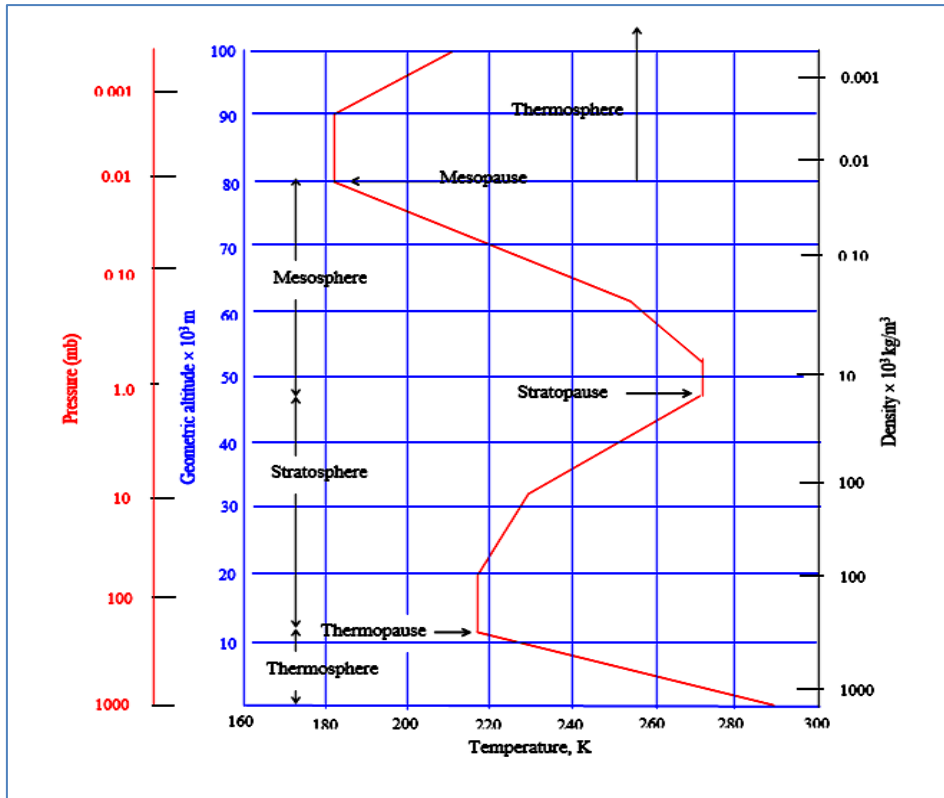**Fig. 2: Flight trajectory of (a) SLV and (b) re-entry of spacecraft**
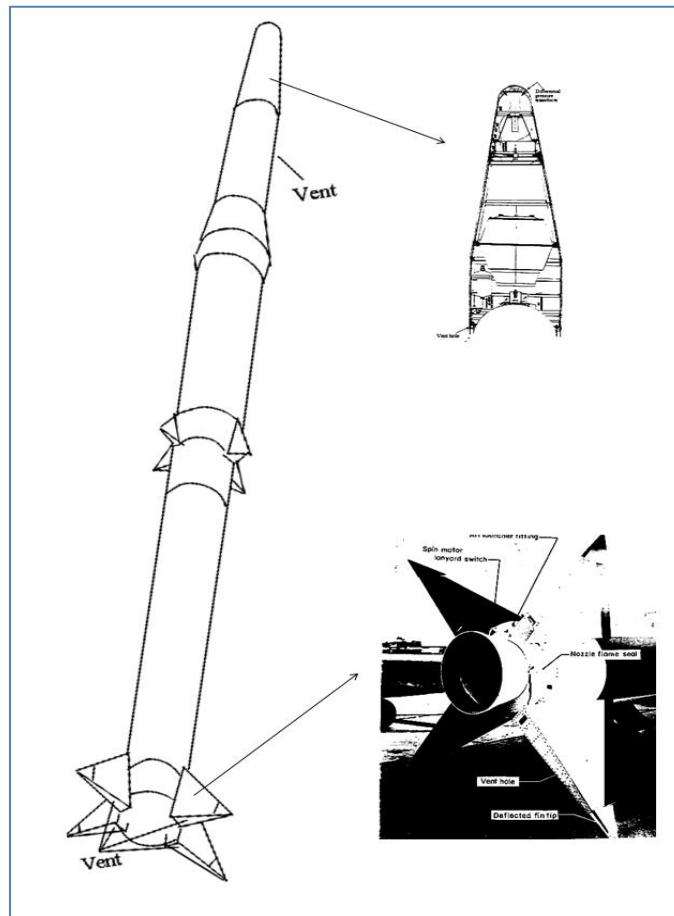
Fig. 3: Earth atmosphere up to 10^5 m

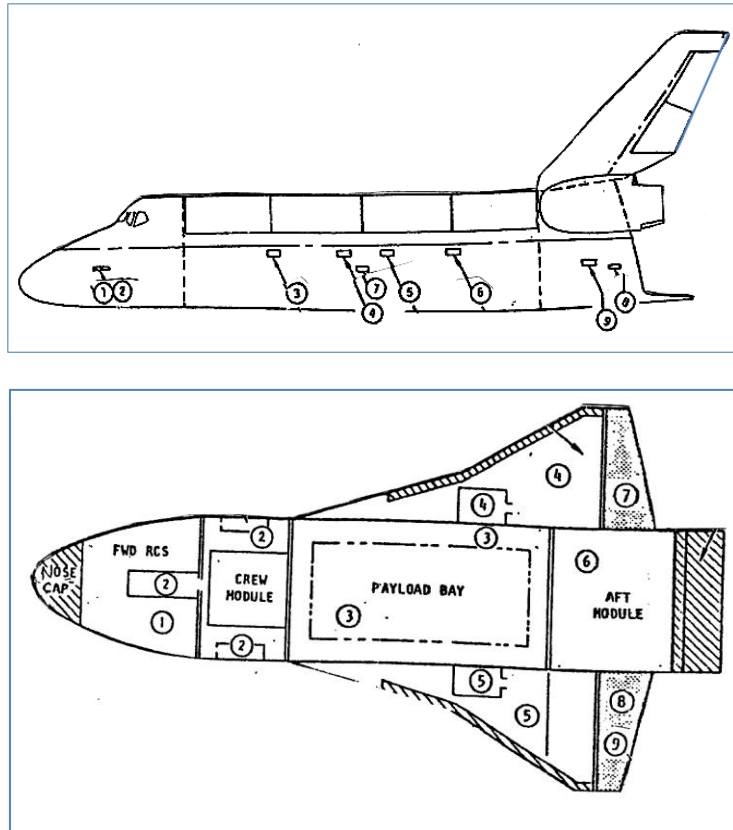
Fig. 4: Vent system over RM B sounding rocket

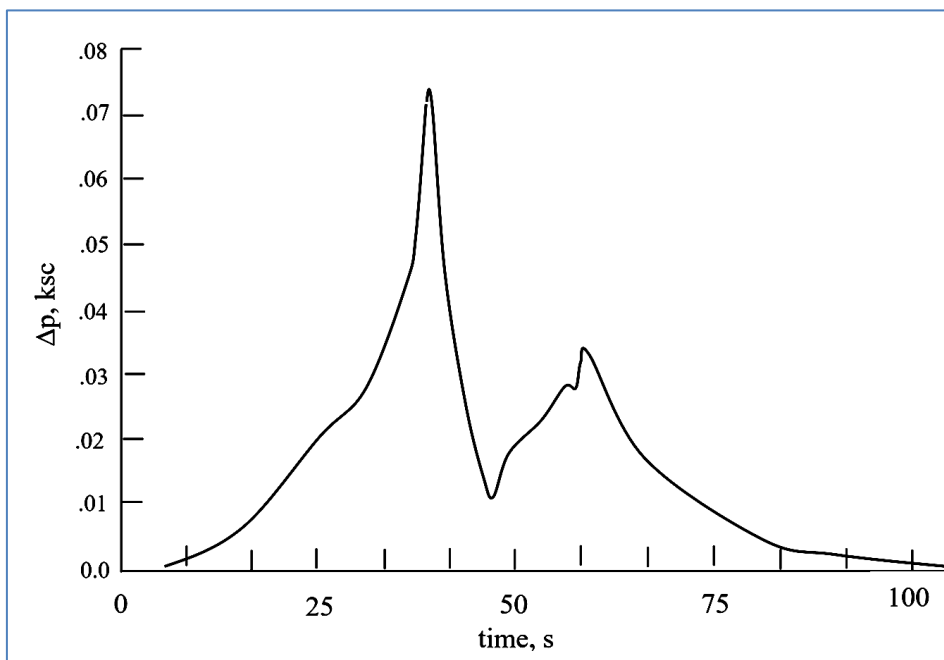**Fig. 5: Various comportment in space shuttle required vent system**
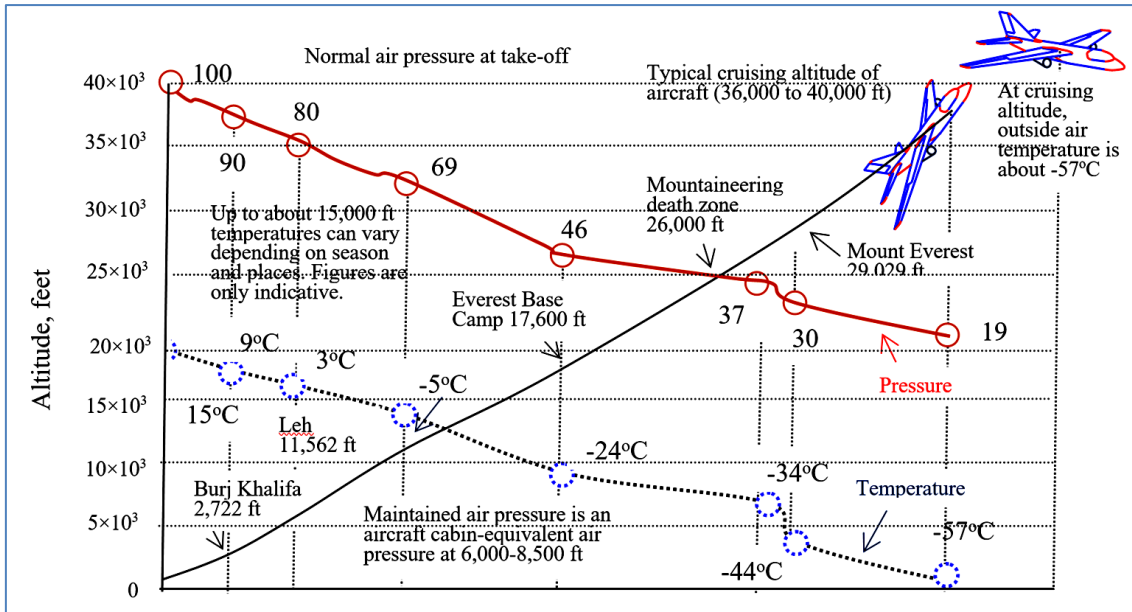

Fig. 6: Variation of differential pressure inside the payload bay
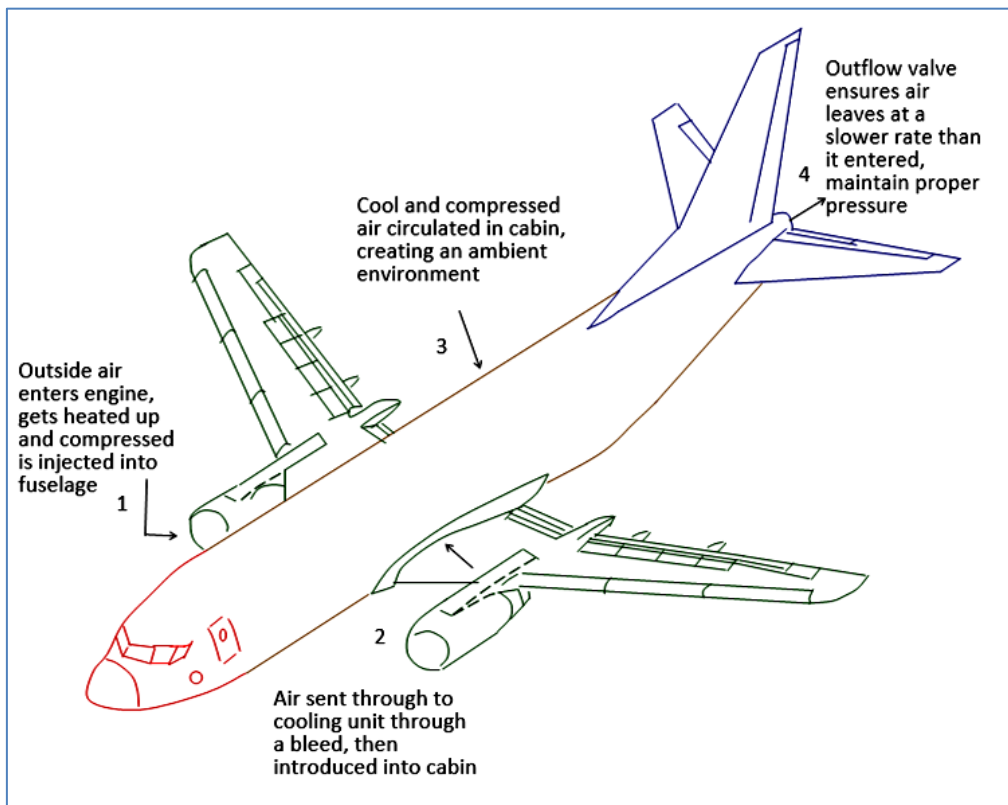
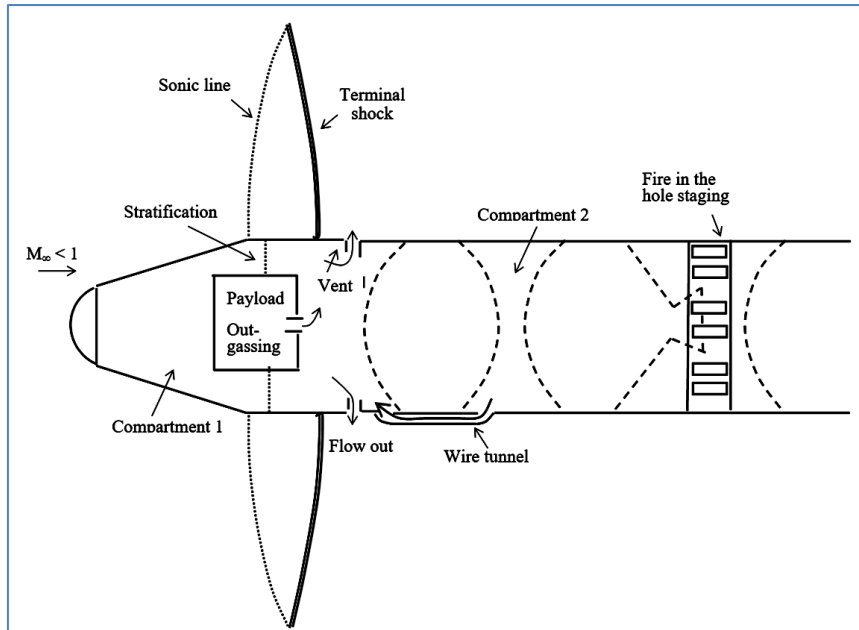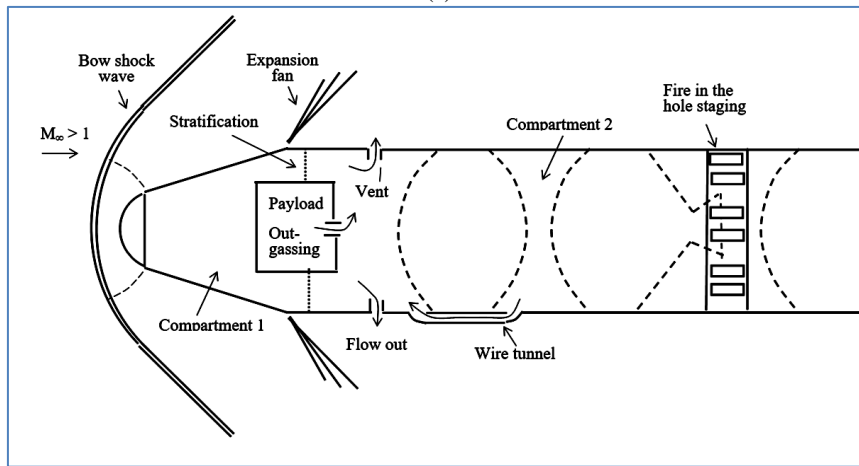**Fig. 7: Variation of pressure, and temperature with altitude**

Fig. 8: Pressurization system of aircraft

(a)

(b)

Fig. 9: Compartment of SLV and Flow field (a) transonic and (b) supersonic speeds
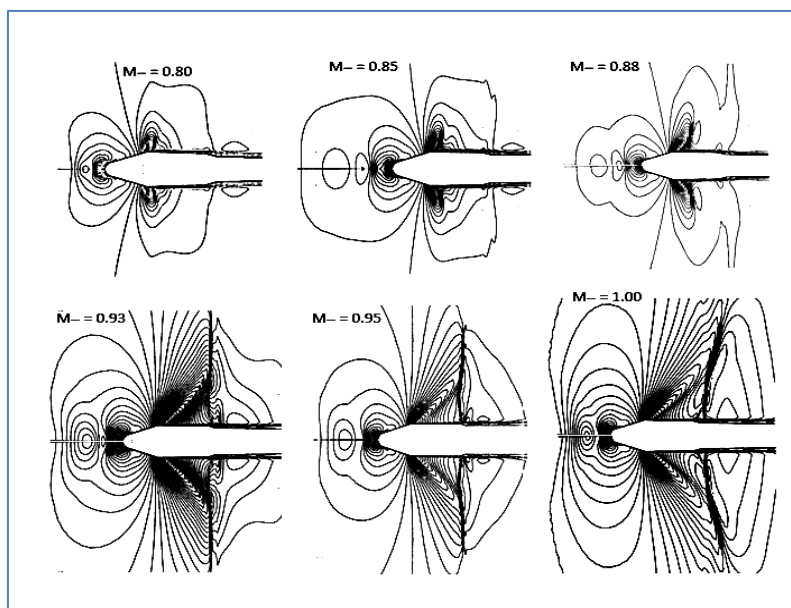
(a)
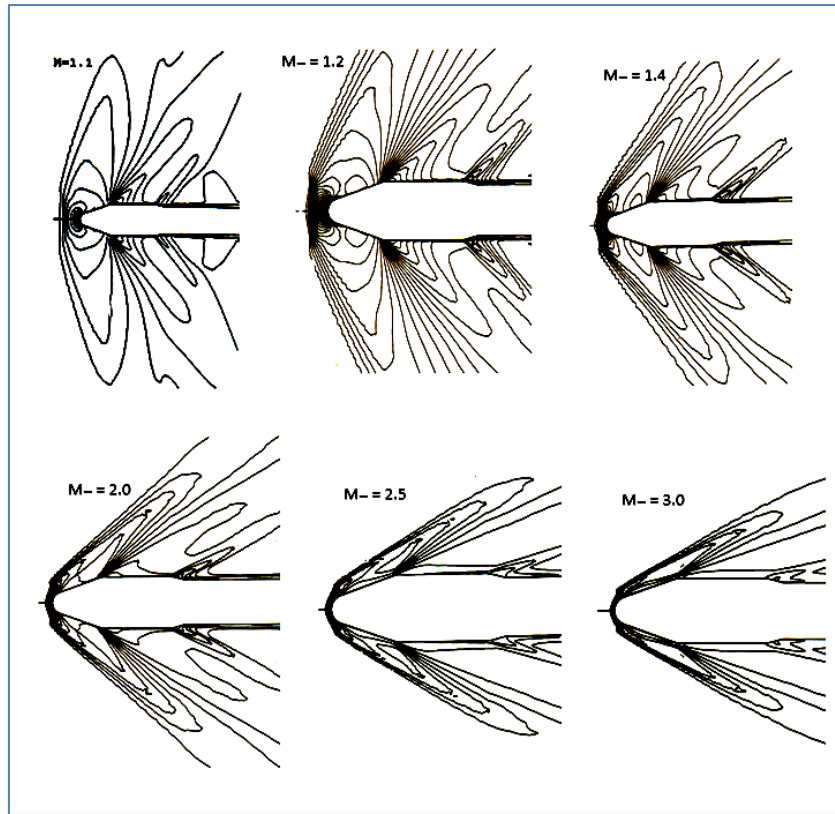
(b)

Fig. 10: Mach contours over SLV at (a) transonic and (b) supersonic speeds
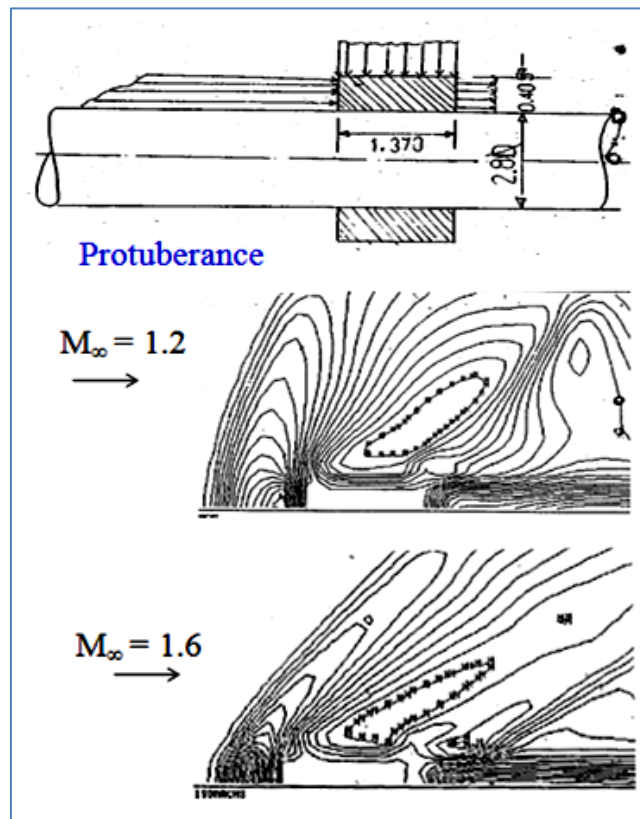
Fig. 11: Flow field over protuberance at Mach 1.2 and 1.6

(a)   (b)
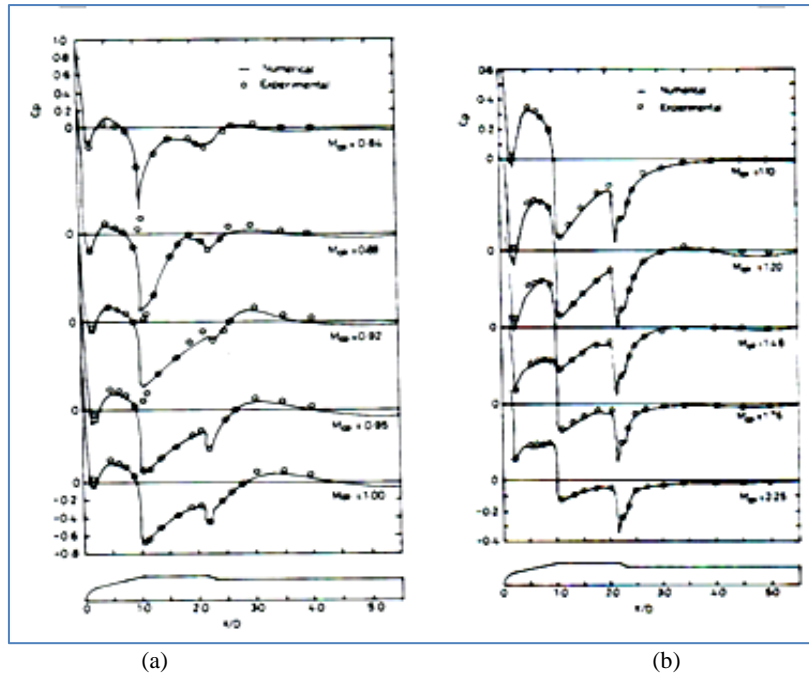
Fig. 12: Variation of pressure over SLV at (a) transonic and (b) supersonic speeds
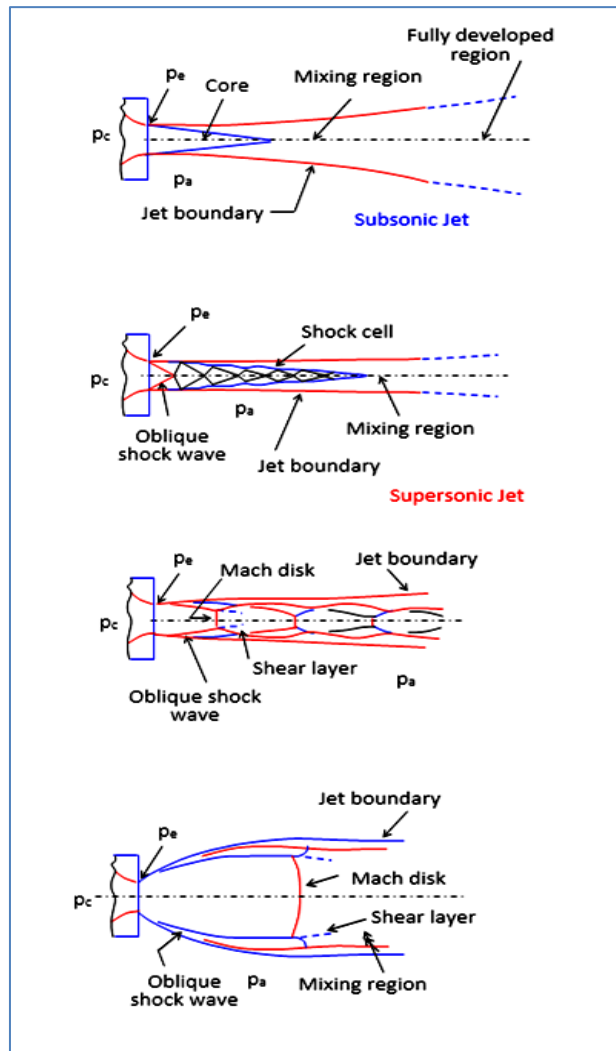
Fig. 13: Jet emanating with increasing pressure ratios, p_b/p_e
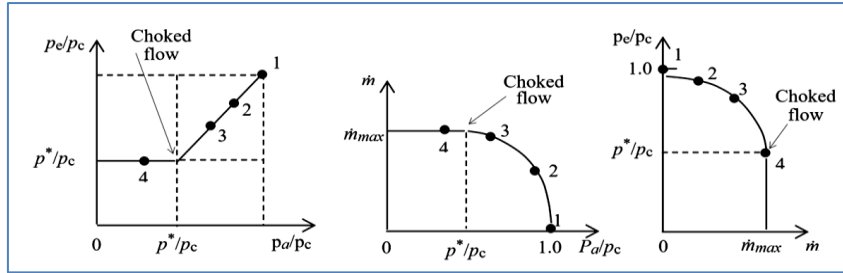
Fig. 14: Pressure and mass flow characteristics
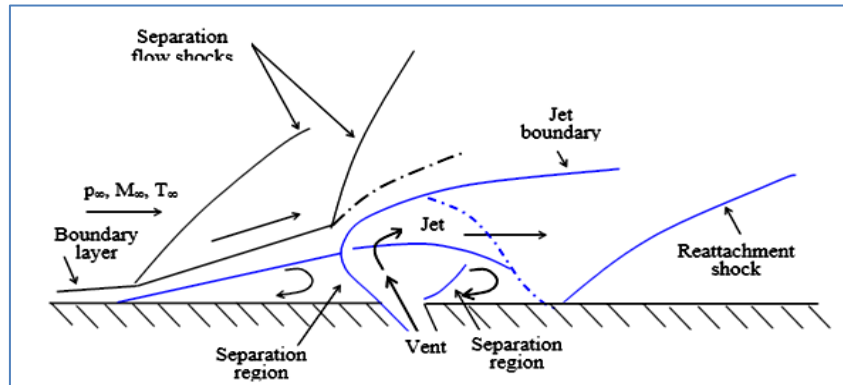
(a)
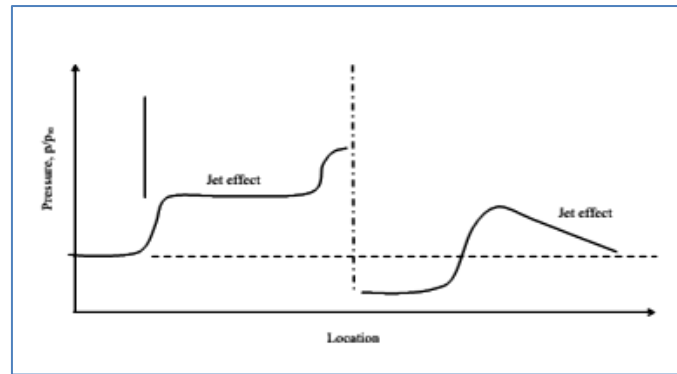
(b)

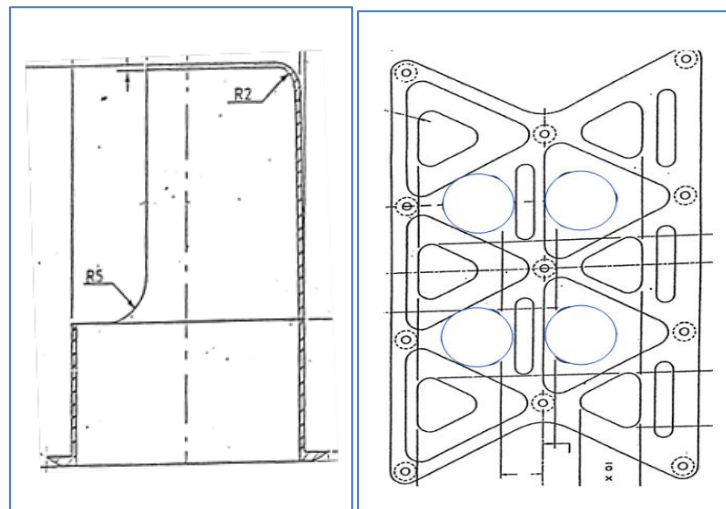**Fig. 15: Schematic sketch of (a) shock wave boundary layer interaction and (b) pressure distribution near vent**

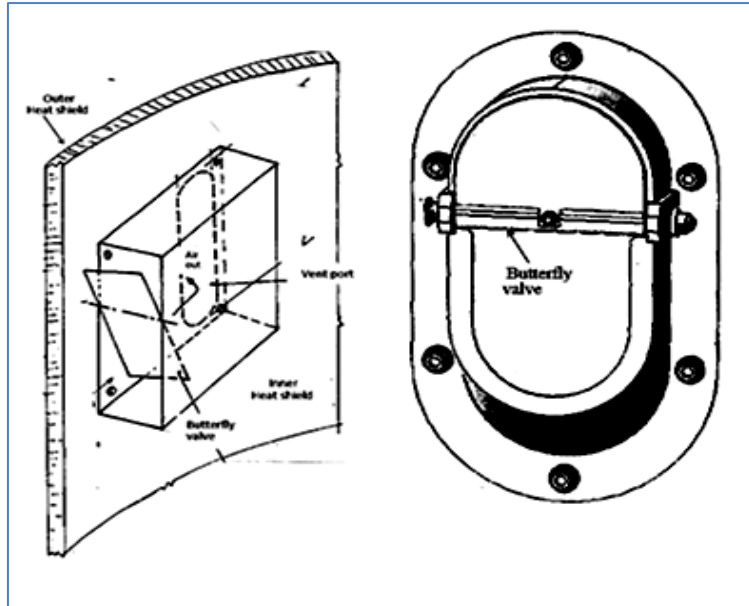
Fig. 16: PLF and vent without valve

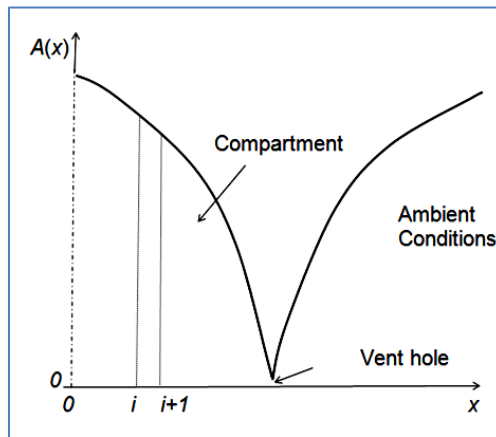**Fig. 17: Various types of butterfly valve**

Fig. 18: Schematic sketch of vent
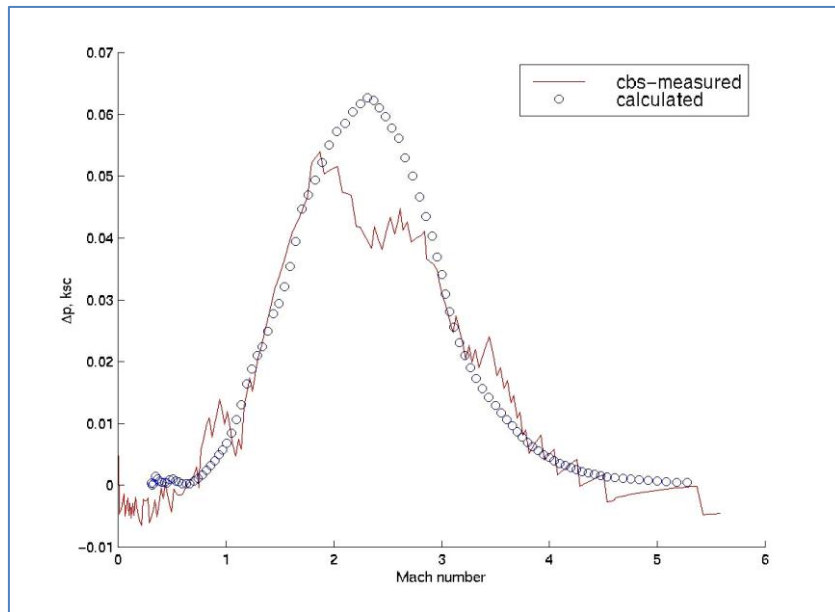

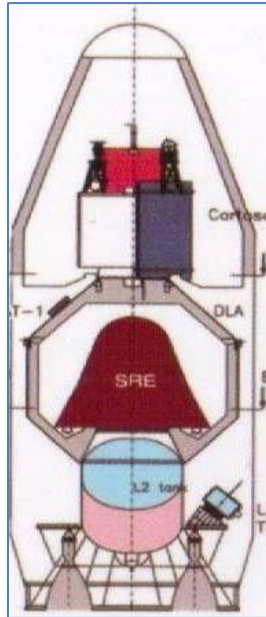**Fig. 19: Computed and measured differential pressure variation inside PLF**

Fig. 20: Spacecraft inside PLF of SLV

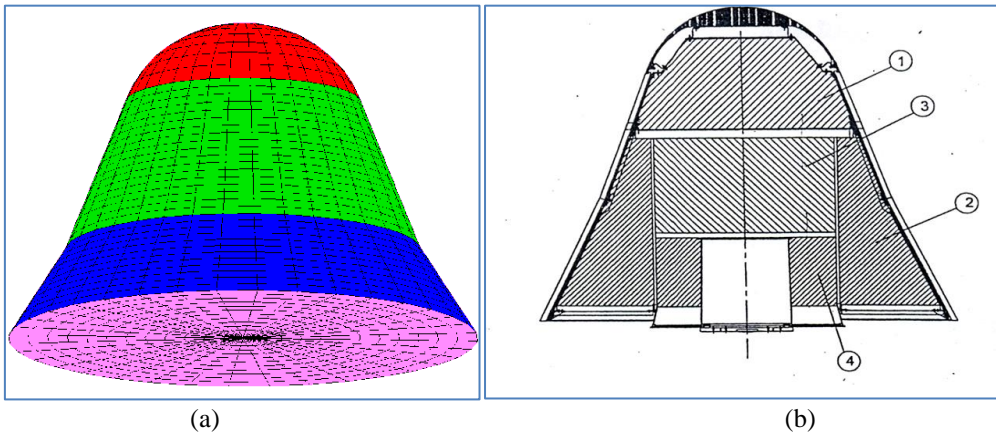(a)   (b)

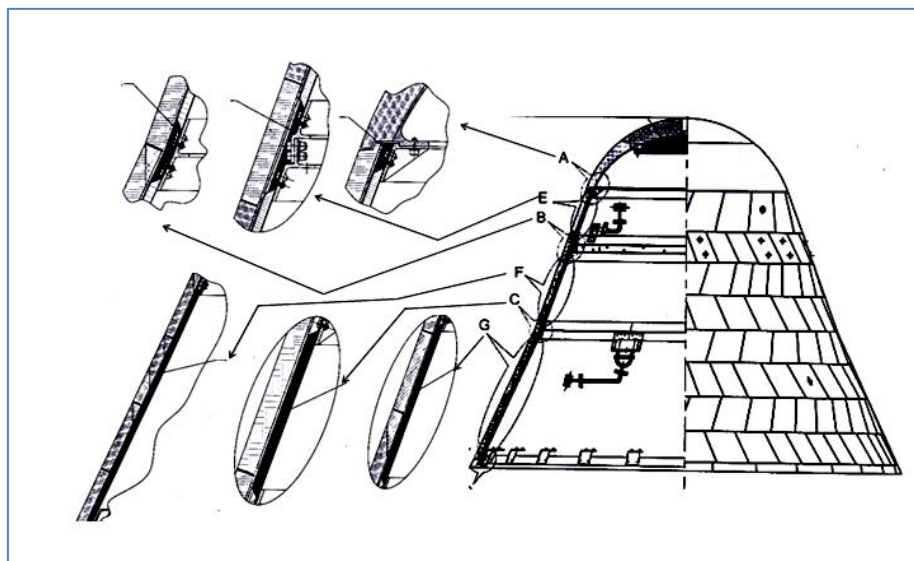**Fig. 21: (a) Spacecraft and (b) compartments of the spacecraft**

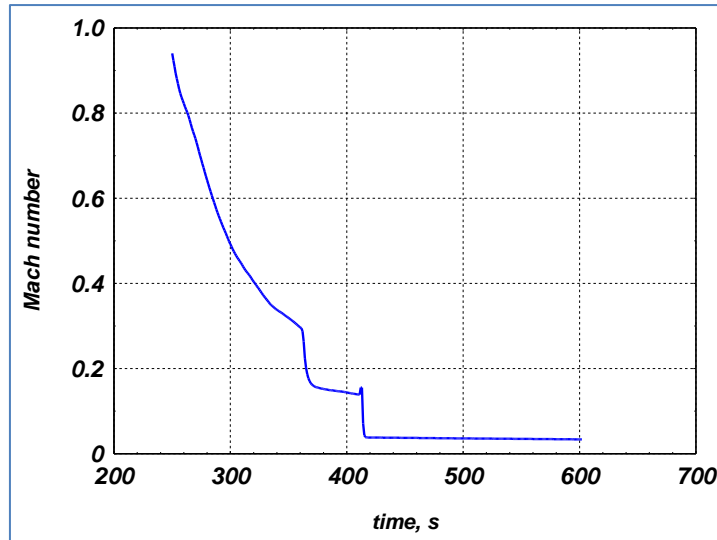**Fig. 22: Honeycomb structure of spacecraft**

Fig. 23: Flight trajectory of re-entry spacecraft
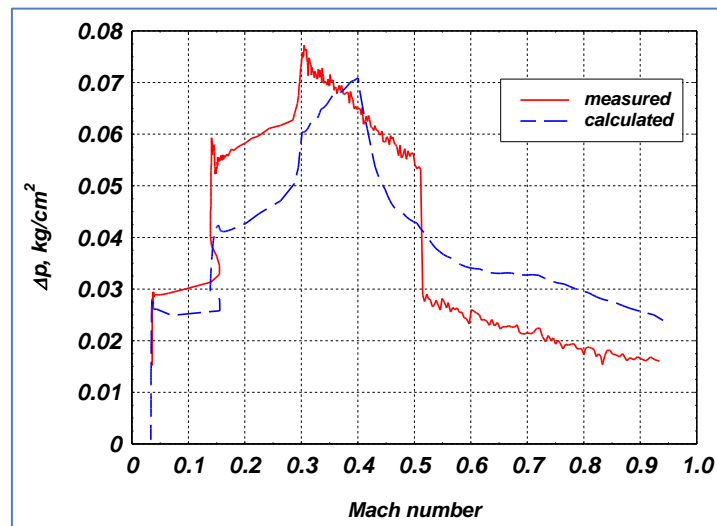

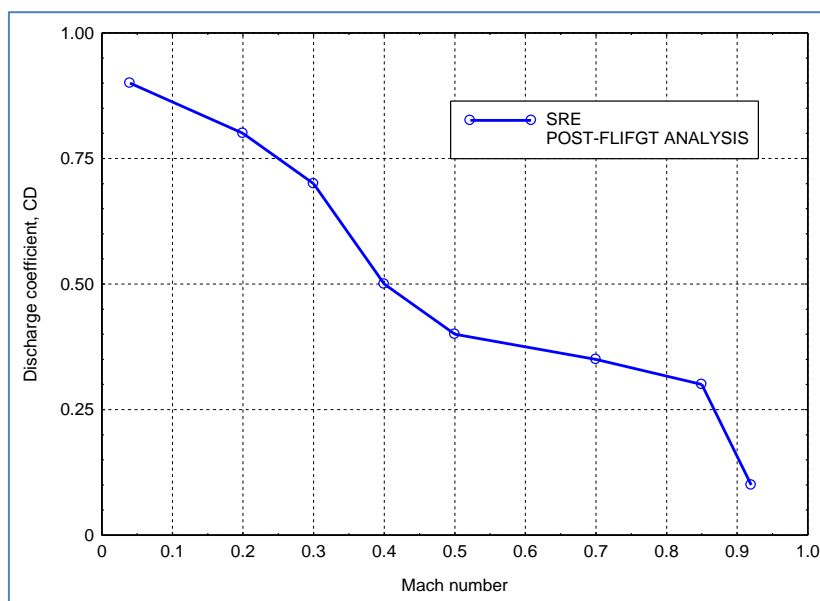**Fig. 24: Computed and measured differential pressure variation inside spacecraft**

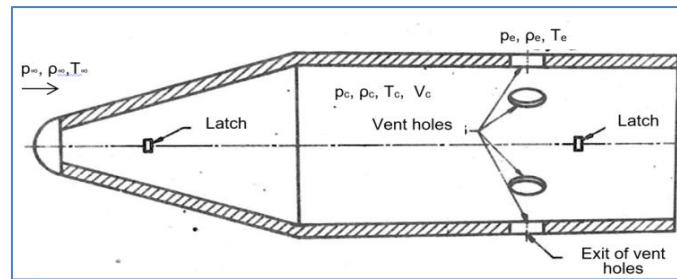**Fig. 25: Estimated discharge coefficient of vent system of spacecraft**

Fig. 26: Structure load on latch

CONCLUSIONS

Space vehicle and spacecraft contains several comportments such as heat shield, payload shroud fairing, base shroud, insulation panels, honeycomb, corrugated structure, whose walls may be subjected to critical loads due to pressure differentials across them. Comportments of SLV are exposed to a decreasing external pressure and may needs a control venting process.

In aircraft, gas dynamics of rapid and explosive decompressions of pressurized aircraft including active venting, physics of rapid decompression, analysis of an aircraft fuel tank venting system

A numerical method based on a direct integration scheme is used for the solution of the non-linear system of ODS's resulting from the analysis of multicompartment of SLV, spacecraft and aircraft. The attention is focused on the modelling of vents within an isentropic model for SLV, spacecraft and aircraft decompression and pressurization. Nonlinear method is described to estimate the discharge coefficient of vent used in space vehicle, spacecraft and aircraft.

REFERENCES

1. Anathasayanam, M. R., & Narsimha, R. (1987). A proposed international tropical reference atmospheric up to 1000 km. *Advances in Space Research*, 7(10), 117-131
2. Isakowitz, S. J., Hopkins, J. B., & Hopkins, J. P., Jr. (eds.) (2004). Payload Accommodation in International Reference Guide to Space Launch Systems, *4th ed., AIAA, Reston*, VA.
3. Anon. (1970). Compartment venting: space vehicle design criteria, *NASA SP*-8060.
4. Kirby, C. E., & Ivy, G. W. (1973). Flow areas for series-parallel compartment venting to satisfy pressure differential requirements. *Journal of Spacecraft and Rockets*, 10(3), 350-351.
5. John, A. L., & Jones, M. L. (1974). Venting characteristics of gaseous helium and nitrogen discharging into a freestream at Mach number from 0.60 to 1.57, *NASA TM X-2995*.
6. Fay, J. F., & Hengel, J. E. (1993). Pressure dither in venting analyses, *AIAA Paper* 93-3014.
7. Sanz-Andres, A., Santiago-Prowald, J., & Ayuso-Barea, A. (1997). Spacecraft launch depressurization loads. *Journal of Spacecraft and Rockets*, 34(6), 805-810.
8. Mehta, R. C. (1999). Comments on Spacecraft launch depressurization loads. *Journal of Spacecraft and Rockets*, 36(1), 152.
9. Dykhuizen, R. C., Gill, W., & Bruskas, L. A. (2009). Depressurization Solutions of vented enclosures during launch. *CAEA Space Journal*, 1(1), 1-6.
10. Huseman, P. G., & Chern, S-Y. (1997). Discharge coefficient analysis for Titan IV payload fairing vents. *AIAA Paper*, 97-2068.
11. Brower, T. L. (2006). Titan launch vehicle; Ground test history. *Journal of Spacecraft and rockets*, 43(1), 147-160.
12. Moraes, P., & Pereira, A. L. (2005). Verification of the pressure equalization inside the satellite compartment of the Brazilian satellite launch vehicle. *J. of the Braz. Soc. of Mech. Sci. & Eng.*, 27(4), 469-472.
13. Mehta, R. C. (2008). Quasi-one-dimensional numerical analysis of payload venting of satellite launch vehicle. *Journal of Spacecraft and Rockets*, 45(2), 412- 414.
14. Pritchett, V. E., Maybe, M. N., Blevins, J. A., Crosby, W. A., & Purinton, D. C. (2014). Aerodynamic tests of the space launch system for database development. *52nd AIAA Aerospace Sciences Meetings*, AIAA 2014-4086.
15. Rogers, S. E., Dalle, D, J., & Chan, W. M. (2015). CFD Simulations of the Space Launch System Ascent Aerodynamics and Booster Separation. *AIAA*, 2015-0778.
16. Iqbal, M. T., & Majid, A. (2018). Design and development of depressurization system of launch vehicle fairing. *Journal of Space Technology*, 8(1), 32-36
17. Benavente, F. M. B. (2015). Thermodynamics study of compartment venting. *Mechanical Engineering department, M. S. thesis, Instituto Superior Tecnico, Lisbon,* Portugal.
18. Oh, T. H., Ko, J. Y., Kim, Y., Lee, J. H., & Ok, K. (2018). Vent valve for test launch vehicle of Korea space launch vehicle-II. *Journal of Spacecraft and rockets*, 55(1), 681-686
19. Singh, K. P. (1979). On the venting of heat shield compartment of a satellite launch vehicle. *Journal of Aeronautical Society of India*, 31(1-4), 93-96

20. Mehta, R. C. (2009). Numerical simulation of depressurization in multi-compartments. *Computational Fluid Dynamics Journal*, **17**(3), 165-172.

21. Mehta, R. C. (2017). Analysis of payload compartment venting of satellite launch vehicle. *Advances in Aircraft and Spacecraft Sciences,* **4**(4), 437-448.

22. Wang, Q., & Arner, S. (2009). Compartment Venting Analysis of Ares I First Stage Systems Tunnel. *AIAA* 2009-5526.

23. Downs, W., Kirchner, R., Hand, L., McLachlan, B., & Nelson, S. (2011). Ares I-X Upper Stage Simulator Compartment Pressure Comparisons during Ascent, Aerospace Sciences Meeting. *AIAA* 2011-1000.

24. Smith, R. N. (2011). Compartment venting on the Orion Crew Module during atmospheric re-entry. *AIAA* 2011-427.

25. Johnson, C. E., Tran, H. K., Smith, M., & Dill, H. (1997). Stardust back shell and back interface plate design verification tests in the NASA Ames arc jet facilities. *AIAA* 97-2483.

26. Charette, R. G., & Yales, E. J. (1980). Base vent assembly for entry space vehicles. *United State Patent 4*, 234,144.

27. Scialdone, J. (1998). Spacecraft compartment venting, NASA Technical Memorandum 4327, *San Diego, California.*

28. Mehta, R. C. (2020). Estimation of discharge coefficient of compartment venting during atmospheric re-entry of the space capsule. *Journal of Aerospace Sciences and Technologies*, 72(1), 41-47

29. Muraca, R. L. (1967), External and internal air loads on sounding rockets. *Journal of Spacecraft and Rockets*, 4(9), 1207-1210.

30. Raper, J. L., Keynton, R. J., & Woodbury, G. E. (1964). Detailed description and flight performance of the RAM B vehicle. *NASA TN D*-2437.

31. Mironer, A., & Regan, F. (1983). Venting of space-shuttle payloads. *AIAA Paper* 83-2600.

32. Murri, B. W. (1987). Payload venting in worst case shuttle environments. *AIAA Paper* 87-1589.

33. Lutfi, H. S., & Nieder, R. L. (1983). Space shuttle orbiter venting - Lesson learned. *NASA CR* 2283.

34. Epstein, G., & Ruth, S. (1997). Honeycomb sandwich structures: Vented versus unvented designs for space systems. *The Aerospace Corporation, EI Segundo, CA, USA*, Report No. SMC-TR-94-02.

35. Ahn, H. (1994). An implicit method for numerically stiff venting problems in honeycomb and other multicell configurations. *AIAA paper*-94-2361.

36. Mavriplis, F. (1963). Decompression of a Pressurized Cabin. *Canadian Aeronautics and Space Journal,* 313–318.

37. Pagani, A., & Carrera, E. (2016). Gas dynamics of rapid and explosive decompressions of pressurized aircraft including active venting. *Advances in Aircraft and Spacecraft Sciences,* 3(1), 77-93.

38. Jensen, D. L. (2000). Analysis of a Boeing 747 Aircraft Fuel Tank Vent System. *AIAA* 2000-2454.

39. Breard, C., Lednicer, D., lachendro, N., & Murvine, E. (2004). A CFD analysis of sudden cockpit decompression. *AIAA Paper* 2004-0054.

40. Daidzic, N. E., & Simones, M. P. (2010). Aircraft Decompression with Installed Cockpit Security Door. *Journal of Spacecraft,* 47(2), 490-504.

41. Mehta, R. C. (2009). Numerical study of flow field visualizations over a payload shroud at transonic speeds. *Journal of Aerospace Engineering*, 223(G), 179-185.

42. Mehta, R. C. (1997). Flow field study over a bulbous payload shroud in transonic and low supersonic Mach number. *AIAA* 97-2256.

43. Mehta, R. C. (2016). Computation of aerodynamic load on protuberance over satellite launch vehicle at supersonic speed. *Scholar Journal of Engineering and Technology*, 4(7), 301-307.

44. Johns, A. L., & Jones, M. L. (1974). Venting characteristics of gaseous helium and nitrogen discharging into a freestream at Mach number from 0.60 to 1.57, *NASA TM X*-2995.

45. Erickson, G. E. (2007). 0.01-Scale CLV DAC-1 Pressure Model Testing at Supersonic Speeds in the NASA Langley Research Centre unitary plan wind tunnel. *NASA Langley Research Centre*.

46. Liepmann, H. W., & Roshko, A. (2007). Elements of gas dynamics. *First South Asian edition, Dover, New Delhi*, pp. 107-109

47. Shapiro, A. H. (1953). The dynamics and thermodynamics of compressible fluid flow. *John Wiley & Sons,* USA, 1, 91-105

48. Saad, M. A. (1985). Compressible fluid flow. *Prentice Hall Inc, NJ,* USA.

49. Jameson, A., Schmidt, W., & Tukel, E. (1981). Numerical simulation of Euler equations by finite volume methods using Runge-Kutta time stepping schemes. *AIAA paper* 81-1259.

50. Gerolymos, G-A., & Geai, P. (1984). Numerical computation of steady and unsteady flows of liquid parahydrogen (LH$_2$). *La Recherche Aerospatiale*, 4, 283-289

51. Price, A. (1978). A controlled random search procedure for global optimization 2. *North-Holland Publishing Co.,* the Netherlands, 71-84.

52. Mehta, R. C., & Tiwari, S. B. (2007). Controlled random search technique for estimation of convective heat transfer coefficient. *Heat and Mass Transfer Journal,* 43, 1171-1177.

53. Mehta, R. C. (2003). Inverse venting problem for estimation of the discharge coefficient in a satellite launch vehicle. *Journal of Aerospace Engineering*, 217(G6), 277-281.